8TH INTERNATIONAL SYMPOSIUM ON PARTICLE IMAGE VELOCIMETRY - PIV09
Melbourne, Victoria, Australia, August 25-28, 2009

Studying the invariants of the velocity-gradient tensor of a round turbulent jet using Tomo-PIV

M.Khashehchi[1], G.E.Elsinga[1], H.Bornstein[2], C.Atkinson[2], A. Ooi[1], Ivan Marusic[1], Julio Soria[2]

[1]Department of Mechanical Engineering,
University of Melbourne, Melbourne, Victoria, 3010, AUSTRALIA
imarusic@unimelb.edu.au
[2]Laboratory for Turbulence Research in Aerospace and Combustion, Department of Aerospace and Mechanical Engineering, Monash University, Clayton, Victoria, 3800, AUSTRALIA
julio.soria@eng.monash.edu.au

ABSTRACT

Turbulence of the round jet has been assessed using invariants of the velocity gradient tensor. Experimental data, obtained using Tomographic Particle Image Velocimetry (Tomo-PIV), using four PCO-4000 cameras with 11 megapixel resolution, is presented for a seeded free air jet, operating in the turbulent regime and the Re number based on the diameter of the nozzle is 10000. Using the acquired 3-D velocity fields, the local statistical and geometrical structure of three-dimensional turbulent flow can be described by properties of the velocity gradient tensor. The invariants of the velocity gradient (R and Q), rate-of-strain (R_s and Q_s), and rate-of-rotation (Q_w) tensors are analyzed across the turbulent expanding regions at different distances from the nozzle outlet. More specifically, the JPDF of invariants is computed, which allows a detailed statistical characterization of the dynamics, geometry and topology of the flow during the entrainment process. It should be noted that the results obtained are indicative of the preliminary work in this area.

1. INTRODUCTION

After more than one century of research, turbulence is still one of the biggest unsolved problems in fluid flows. The round jet has played a key role in turbulent research since the early work of Liepmann and Laufer[1]. The basic aim of control strategies in the round jet is to evaluate the large scale coherent structures outlined by Burattini [2]. These vortical structures play a major role in transporting mass, heat and momentum in the near field of a jet. Coherent structures result from the initial jet instability (laminar region in this paper) through the selective amplification of small disturbances.
A fundamental link between the mechanisms of creating coherent structures and initial conditions is not clear. One possibility is to assess transitional region of the jet which is the region between the near-field, where the flow is dominated by a laminar one dimensional structure and the fully turbulent self-similar region which contains vortical structures. In the transitional region of the turbulent jet, as a result of small disturbances in the mean flow, the vorticity vectors have broken into highly complex structures. In this region it may be possible to observe the evolution of the turbulence into the self similar region and interactions due to vortex dynamics.

1-1-*Method Of Velocimetry*

Evaluating the statistical properties of the spatially developing turbulence requires a technique that can resolve the instantaneous three dimensional flow field, with the proper resolution to obtain reliable statistics. Recently, Elsinga (2007)[3] described the tomographic particle image velocimetry technique (Tomo-PIV) that is capable of measuring all three velocity components in a three-dimensional volume. The technique makes use of several simultaneous views of the illuminated particles and utilises 3D reconstruction of light intensity distribution by means of optical tomography. These reconstructive techniques are also outlined by Atkinson and Soria[4].

1-2-*Study of VGT*

The study of the invariants of the velocity gradient, rate-of-strain, and rate-of-rotation tensors in turbulent flows has been introduced first by Cantwell, Chong et al.[5], [6-7] and [8]. The invariants are scalar quantities whose values are independent of the orientation of the coordinate system and contain information concerning the rates of vortex stretching and rotation, and on the topology and geometry of deformation of the infinitesimal fluid elements. Furthermore, the analysis of the invariants permits the understanding of these issues using a relatively small number of variables. The invariants have been extensively used in several flow configurations such as isotropic turbulence seen in work by Martín, Nomura and Post, Ooi [9-11], turbulent mixing layers investigated by Soria [12] and turbulent channel flows described by Blackburn et al.[13]. Important information is also obtained by analysing the volume integral of the invariants, as shown by Soria et al.[14] In these studies, several "universal" features of turbulent flows were observed. An example of such a result is the well known "teardrop" shape of the joint probability density function (JPDF) of R and Q. Another area of research involving the invariants has been the identification of the coherent structures in turbulent flows, either to visualize the flow regions associated with the presence of vortex tubes which has been performed by Dubief and Delcayre [15] or to identify the regions responsible for the most important dissipation rates of kinetic energy as discussed by Horiuti[16-17].
This paper represents a first attempt to measure, with Tomo-PIV, the development of turbulence from laminar region through the transitional region of a round jet and analyse the evolution of the invariants of the velocity gradient tensor.

Field Code Changed

2-Invariants of the Velocity Gradient, Rate-of-Strain and Rate-of-Rotation tensors

A brief review of the definitions of the invariants is presented below. The interpretation of these invariants, defined by their relation to the physical properties of the flow has been studied by Chong et al. (1990) Ooi et al. (1999) and Da Silva (2008) among others[18]. This analysis uses Joint Probability Distribution Functions (JPDF's) of the invariants at several distances from the outlet of the jet.

The velocity gradient tensor $A_{ij} = \frac{\partial u_i}{\partial x_j}$ can be decomposed into a symmetric (rate-of-strain) and a skew-symmetric (rate-of-rotation) component, $A_{ij} = S_{ij} + W_{ij}$ and has the following characteristic equation:

$$\lambda_i^3 + P\lambda_i^2 + Q\lambda_i + R = 0 \quad (1)$$

Where λ_i are the Eigen values of the A_{ij} . P, Q and R are the first, second, and third invariants of the velocity gradient tensor respectively and define by:

$$P = -A_{ii} \quad (2)$$

$$Q = -\frac{1}{2} A_{ij} A_{ji} \quad (3)$$

$$R = -\frac{1}{3} A_{ij} A_{jk} A_{ki} \quad (4)$$

Similarly, the invariants of the rate-of-strain tensor are defined by its characteristic equation. The independent invariants of S_{ij} are:

$$Q_s = -\frac{1}{2} S_{ij} S_{ji} \quad (5)$$

$$R_s = -\frac{1}{3} S_{ij} S_{jk} S_{ki} \quad (6)$$

In the rate-of-rotation tensor third invariant is zero and second one is defined by following equation:

$$Q_w = -\frac{1}{2} W_{ij} W_{ji} \quad (7)$$

For incompressible flows $P = P_s = 0$ due to continuity.
The invariants defined above are usually analysed in the form of joint PDFs combining two invariants. The most common combinations consist on the JPDF of (R, Q), (R_s, Q_s) and $(Q_w, -Q_s)$.

3-Experimental setup

Tomo-PIV has been applied to an axi-symmetric air jet to find 3D velocity distribution at different distances from the nozzle exit. The nozzle is 2mm in diameter and is mounted on bearings which attach to a rail allowing translation in the vertical plane. The seeding material used is a Water-Based solution containing 12g/L of sugar. This solution is vaporised by an Ultrasound device (APC Nebuliser) with particles that average 2μm in diameter.

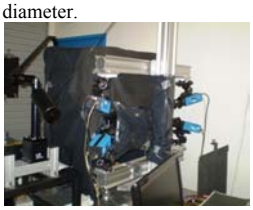

Figure 1. Experimental Tomo-PIV setup

For the Tomo-PIV experiments 4, PCO4000 cameras (4008×2672 pixels) are used. They are positioned such that all 4 cameras are operating in forward scatter with X-95 rails used to mount 2 cameras looking at an angle of 10° down on the jet, while the other 2 cameras look at the same angle upwards towards the jet. All cameras are at an angle of 25° from the angle perpendicular to the direction of the light sheet, Fig. 1.

Field Code Changed

Illumination of the particles is provided by a New Wave Nd-Yag laser that emits at the 512nm wavelength. The Δt value used for the experiments was (0.01 ms). The light sheet was 5mm thick at the jet.

In order to have background seeding in the outer flow, in addition to the seeded jet, a tent was placed over the setup to confine the seeding particles. This background seeding is required to measure the velocity in the entrainment region of the flow.

The camera calibration device was mounted on bearings that fitted onto the same rails as the jet giving it vertical movement and was mounted on a micrometer allowing horizontal motion. The calibration grid itself was a black transparency with white dots that was used in order to place all cameras in forward scatter.

The recorded particle images were analysed using the DaVis software from LaVision GmbH. The 3-D intensity distribution was reconstructed using the MART algorithm with 5 iterations [3] at a spatial resolution of 110 voxels/mm. The correlation volume size was 40^3 voxels, using a 50% overlap resulted in a vector spacing of 0.18mm in each direction (Fig 2a). The image shown in Figure 2b, provides a reconstruction of a sub-region from x/d = 0-4 with better spatial resolution. The interrogation windows are 64 voxels in size and there is a 75% overlap.

4-Results

An example of a measured three-dimensional velocity field consisting of 44x44x6 vectors (a subregion of the complete measurement domain) is shown in Fig.2.

Field Code Changed
Field Code Changed
Field Code Changed

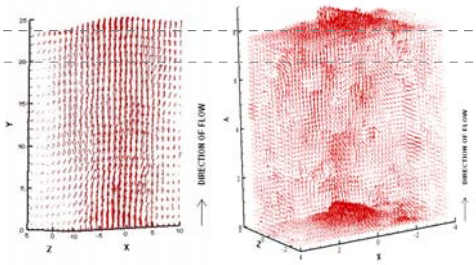

Figure 2. a) Three-dimensional velocity field measurement for x/d = 0-15 **b)** Three-dimensional velocity field measurements x/d = 0-4

Iso-contours of velocity field in stream-wise direction (dominated direction in the jet) measured by Tomo-PIV for three different distances from outlet of the jet are shown in Figure 4

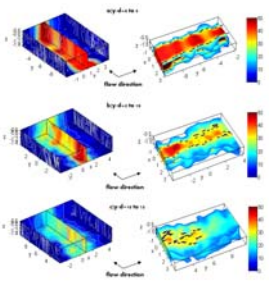

Figure 4. Iso-contour of stream-wise velocity component (a) $\frac{y}{d}$=0 to 5 (b) $\frac{y}{d}$=5 to 10 and c) $\frac{y}{d}$=10 to 15.

4-1-Analysis of the invariants Q_w and Q_s

In this section, analysis of the second invariants of the rate-of-strain and rate-of-rotation tensors Q_w and Q_s, across the stream-wise direction are performed in order to analyse the local geometry of the dissipation field.
The different physical interpretation for various regions of the joint PDFs of Q_w and Q_s is shown in Fig. 6.

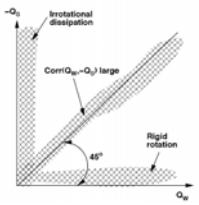

Figure 6. Physical interpretation of various regions in the Q_w vs $-Q_s$

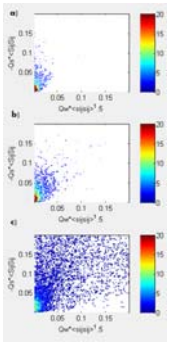

Figure 7. JPDF of instantaneous invariants of Q_w vs $-Q_s$ for three different distances from the outlet of the jet (a) $\frac{y}{d}$=0 to 5 (b) $\frac{y}{d}$=5 to 10 and c) $\frac{y}{d}$=10 to 15

Following common practice, the invariants Q_w and Q_s were non-dimensionalised with $\langle S_{ij}S_{ij}\rangle$ in Fig 7.

In the preliminary result at the laminar region, Fig 7a , the JPDF of (Q_w,$-Q_s$) shows a slight tendency to be aligned with the vertical line defined by Q_w=0. This shows a strong predominance of dissipation over enstrophy. Later on in the evolution of the flow, Fig 7b and 7c (left), the joint PDF shows a stronger correlation between Q_w and $-Q_s$, hence strong enstrophy coexists with strong strains. This is due to the formation of stronger coherent structures in the evolution of the jet.

4-2-Analysis of the invariants Q_s and R_s

In this section, the second and third invariants of the rate-of-strain tensor Q_s and R_s have been used in order to analyse the geometry of straining of the fluid elements.
The evolution of the joint PDFs of R_s vs. Q_s is shown in Fig 8. Because of the symmetry of S, the data falls below the discriminant line (D=0) which is defined by:

$$D = 27R^2 + 4Q^3 \qquad (9)$$

It can be seen that at laminar region ($\frac{y}{d}$=0 to 5), the joint PDFs show a strong tendency towards the line D= 0 and as the flow move from the jet outlet, the magnitude of Q_s and R_s grows, moving away from D=0. The three joint PDFs all show a clear preference for the region R_s and Q_s<0 associated with extensive straining of the fluid elements. The apparent excursions above discriminant line that can be seen in Figure 8 are the result of interpolation errors by the plotting software.

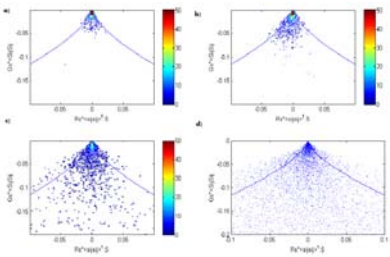

Figure 8. Contour plot of JPDF of non-dimensional invariants of the rate of strain tensor (a) y/d = 0 to 5 (b) y/d=5 to 10 c) y/d=10 to 15 and d) distribution of points in the Q_s and R_s plane

4-3-Analysis of the invariants Q and R

This section analyses the second and third invariants of the velocity gradient tensor Q and R in order to analyse the relation between the flow topology and dynamics. The first important observation concerns the general shape of the JPDFs. At the laminar and transient regions shown, the teardrop characteristic shape of the (Q and R) phase map cannot be seen yet by preliminary result shown in Fig. 9.
The preliminary work, utilising higher resolution in the laminar region near the nozzle is shown in Fig. 10.
The values of R and Q exist only below the lines defined by the discriminant D=0 (Fig 9). This is consistent with the results described before, i.e., at the outlet of the jet, strain product dominates over enstrophy and thus Q<0.

In the first region the joint PDF is shaped like a “crescent” with preference for D< 0, hence points in the flow field have a preference for the local topology UN/S/S and SN/S/S,

indicating that regions in the flow are undergoing contraction. As the flow evolves, there is a preference for SF/S, hence the focal regions in the flow are being stretched.

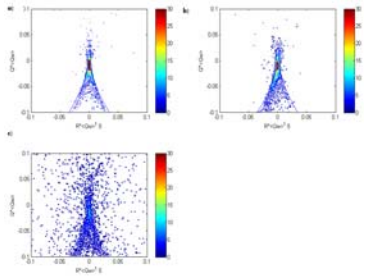

Figure 9. Contour plot of JPDF of the invariants of VGT: (a) $\frac{y}{d}$=0 to 5 (b) $\frac{y}{d}$=5 to 10 and c) $\frac{y}{d}$=10 to 15

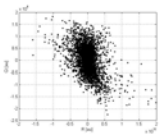

Figure 10. Plot of Q-R JPDF of non-dimensional invariants of the velocity gradient tensor for x/d = 0-4 (High Resolution)

In addition to the Q-R plot shown for the higher resolution near the nozzle a Q iso-surface was extracted and shown in Figure 11. This Q isosurface shows a solid core with a helical/horseshoe structure encompassing the core of the flow.

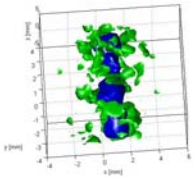

Figure 11: Q Iso-surface of Volume from x/d=0-4

5-CONCLUSIONS

From these preliminary results, the invariants of the velocity gradient (R and Q), rate-of- strain (R_s and Q_s), and rate-of-rotation (Q_w) tensors were analysed near the outlet of the jet for a Reynolds Number of 1000.

The joint PDF of Q_w and $-Q_s$ shows that at the outlet, all the flow points are characterized by irrotational dissipation, i.e., there is still no sign of the coherent vortices that are known to exist in the turbulent region. The analysis of the invariants R and Q show that the classical teardrop shape of the (R, Q) phase map has not yet formed in the region analysed.

The invariants, Q_s and R_s, which are proportional to the viscous dissipation rate and strain skewness, respectively, also increase within this region, although at a smaller rate.

Indeed, these invariants should only reach their turbulent values long after the point of $\frac{y}{d}$=20 (self similar region of jet). This is only preliminary work and future work will analyse the invariants of the VGT in the self similar region.

References

1. Liepmann, H., J. Laufer, and Investigation of free turbulent mixing. NACA Tech Note, 1947: p. 1258.
2. Burattini, P., et al., Effect of initial conditions on the near-field development of a round jet. Exp Fluids, 2004. **37**: p. 56-64.
3. Elsinga, G., et al., Tomographic particle image velocimetry. Exp Fluids, 2006. **41**: p. 933-947.
4. Atkinson, C. and Soria, J.. "Efficient simultaneous reconstruction and direct cross-correlation techniques for tomographic particle image velocimetry." Exp Fluids In Press
5. Chong, M., E. Perry, and B. Cantwell, A general classification of three dimensional flow fields simulations of turbulence. Phys. Fluids A, 1990. **2**: p. 765.
6. B. Cantwell et. al. Exact evolution of a restricted Euler equation for the velocity gradient tensor. Phys. Fluids A, 1992. **4**: p. 782.
7. Cantwell, B., On the behavior of velocity gradient tensor invariants in direct numerical simulations of turbulence. Phys. Fluids A, 1993. **5**: p. 2008.
8. Perry, A. and M. Chong, Topology of flow patterns in vortex motions and turbulence. Appl. Sci. Res, 1994. **53**: p. 357.
9. Martín, J., et al., Dynamics of the velocity gradient tensor invariants in isotropic turbulence. Phys. Fluids A, 1998. **10** :p. 2336.
10. Nomura, K. and G. Post, The structure and dynamics of vorticity and rate of strain in incompressible homogeneous turbulence. J. Fluid Mech, 1998. **377**: p. 65.
11. Ooi, A., et al., A study of the evolution and characteristics of the invariants of the velocity-gradient tensor in isotropic turbulence. J. Fluid Mech, 1999. **381**: p. 141.
12. Soria, J., et al., A study of the fine-scale motions of incompressible time-developing mixing layers. Phys. Fluids A, 1994. **6**: p. 871.
13. Blackburn, H., N. Mansour, and B. Cantwell, Topology of fine-scale motions in turbulent channel flow. J. Fluid Mech, 1996. **310**: p. 269.
14. Soria, J., A. Ooi, and M. Chong, Volume integrals of the QA−RA invariants of the velocity gradient tensor in incompressible flows. Fluid Dyn. Res, 1997. **19**: p. 219.
15. Dubief, I. and F. Delcayre, On coherent-vortex identification in turbulence. J. Turbul, 2000. **1**: p. 11.
16. Horiuti, K., A classification method for vortex sheet and tube structures in turbulent flows. Phys. Fluids A, 20.13 .01
17. Horiuti, K. and Y. Takagi, Identification method for vortex sheet structures in turbulent flows. Phys. Fluids A, 2005. **17**: p. 121703.
18. Da-Silva, C.B. and J.C.F. Pereira, Invariants of the velocity-gradient, rate-of-strain, and rate-of-rotation tensors across the turbulent/nonturbulent interface in jets. Phys. Fluids, 2008. **20**: p. 055101.